Electronic Journal of Biotechnology 59 (2022) 94–106

Contents lists available at ScienceDirect

Electronic Journal of Biotechnology

www.elsevier.com/locate/ejbt

Research Article

Induction temperature impacts the structure of recombinant HuGM-CSF inclusion bodies in thermoinducible *E. coli*

Sara Restrepo-Pineda [a], Diego Rosiles-Becerril [a], Angélica B. Vargas-Castillo [a,b], Luis P. Ávila-Barrientos [a,c], Axel Luviano [c], Nuria Sánchez-Puig [c], Enrique García-Hernández [c], Nestor O. Pérez [d], Mauricio A. Trujillo-Roldán [a,e], Norma A. Valdez-Cruz [a,*]

[a] *Programa de Investigación de Producción de Biomoléculas, Departamento de Biología Molecular y Biotecnología, Instituto de Investigaciones Biomédicas, Universidad Nacional Autónoma de México, CP 04510 Ciudad de México, Mexico*
[b] *INSERM UMR-S-MD 1197, Hôpital Paul Brousse, Villejuif, France*
[c] *Instituto de Química, Universidad Nacional Autónoma de México, Ciudad Universitaria, Ciudad de México 04510, Mexico*
[d] *Probiomed S.A. de C.V. Planta Tenancingo, Cruce de Carreteras Acatzingo-Zumpahuacan SN, Tenancingo, Edo., C.P. 52400 de México, Mexico*
[e] *Unidad de Bioprocesos, Instituto de Investigaciones Biomédicas, Universidad Nacional Autónoma de México, CP 04510 Ciudad de México, Mexico*

GRAPHICAL ABSTRACT

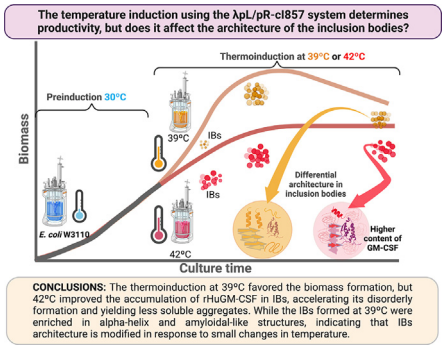

ARTICLE INFO

Article history:
Received 2 January 2022
Accepted 9 August 2022
Available online 13 August 2022

Keywords:
Acetate
Aggregation
Biomass
Bioprocesses
Escherichia coli
Inclusion bodies
Induction
Recombinant human granulocyte–

ABSTRACT

Background: The temperature upshift has been widely used as an induction system to produce recombinant proteins (RPs). However, thermoinduction could affect bacterial metabolism, RP production, and RP aggregation. Understanding the structure and functionality of those aggregates, known as inclusion bodies (IBs), is a research area of interest in bioprocesses being scarcely studied under thermoinduction. Here, we describe the effect of the thermoinduction (39°C or 42°C) on the production of the recombinant human granulocyte–macrophage colony-stimulating factor (rHuGM-CSF) using *Escherichia coli* W3110 under the system λ*pL*/cI857.

Results: Results indicated that at 39°C, the production of biomass was almost doubled as well as the acetate accumulation compared to 42°C. Cultures thermoinduced at 42°C improved 1.5-fold the total protein over biomass yield and 1.25-fold the RP over total protein yield. Furthermore, 42°C accelerated the onset of IB formation, changing its architecture. Additionally, IBs formed at 42°C were less soluble and presented higher disorderly structures compared with IBs formed at 39°C, enriched in α-helix and amyloidal-like structures.

Peer review under responsibility of Pontificia Universidad Católica de Valparaíso

* Corresponding author.
E-mail addresses: sarestrepo90@gmail.com (S. Restrepo-Pineda), hbeckful@gmail.com (D. Rosiles-Becerril), berenicevargascastillo@gmail.com (A.B. Vargas-Castillo), lpablo.ab@gmail.com, lpablo@comunidad.unam.mx (L.P. Ávila-Barrientos), christian_axlj@hotmail.com, aluviano@ifc.unam.mx (A. Luviano), nsanchezpuig@gmail.com, nuriasp@unam.mx (N. Sánchez-Puig), egarciah@unam.mx (E. García-Hernández), nestor.perez@probiomed.com.mx, noperezr@gmail.com (N.O. Pérez), maurotru@iibiomedicas.unam.mx, maurotru@gmail.com (M.A. Trujillo-Roldán), adri@iibiomedicas.unam.mx, adrivaldez1@gmail.com (N.A. Valdez-Cruz).

https://doi.org/10.1016/j.ejbt.2022.08.004

macrophage colony-stimulating factor
Recombinant proteins
Temperature upshift
Thermoinduction

Conclusions: This study highlights the observation that IBs attain different architecture in response to small changes in environmental conditions, such as the induction temperature, being this helpful information to improve thermoinduced bioprocesses.

How to cite: Restrepo-Pineda S, Rosiles-Becerril D, Vargas-Castillo AB, et al. Induction temperature impacts the structure of recombinant HuGM-CSF inclusion bodies in thermoinducible *E. coli*. Electron J Biotechnol 2022;59. https://doi.org/10.1016/j.ejbt.2022.08.004.

1. Introduction

The bacteria *E. coli* has been used as the cellular platform to produce a variety of recombinant proteins (RPs) [1]. Soluble or insoluble RPs can be obtained during overproduction in bacteria [1,2]. RPs incorrect folding can promote self-aggregation in conjunction with endogenous proteins to form self-assembled aggregates known as inclusion bodies (IBs). Factors such as the selected RP, strain, plasmid, inductor concentration, culture time, pH, bacterial growth rate, feeding culture strategies, agitation, and temperature could affect the IB formation, composition, and architecture [3,4,5,6,7,8]. In general, IBs are refractile and dense particles, with diameters between 0.2 and 1.2 μm, presenting semi-spherical or cylindrical structures with crossed β sheets, amyloid fibers, and partial helix or coiled-coil structures [9]. The formation of IBs in bioprocesses is considered a bottleneck for the recovery and purification of RPs. However, IBs are the raw material for the RP downstream processes in biopharmaceutical production [6,9,10]. The IB structure, amyloid content conformation, and the relationship of RP concerning endogenous proteins are essential determinants for the efficient recovery of RP from aggregates, its solubilization, purification, and refolding [11,12,13]. Therefore, the study of the IB architecture has become an important task due to their potential to increase RP recovery that offers the opportunity to simplify the downstream processing in sectors such as health, bioremediation, and the food industry, among others [6,14,15,16,17].

The temperature inducible promoters *pL* and *pR* of the bacteriophage λ are strong and regulated through the temperature-sensitive repressor cI857 [18,19]. The cI857 exerts repression of these promoters below 37°C, while an increase up to 38°C induces a conformational change that allows the transcription of the gene downstream of the *pL* or *pR* promoter [18,19]. Commonly, 42°C has been used to induce the expression of different RPs produced in *E. coli* [18,19]. Thermoinduction avoids the addition of chemical inducers, high productivity is achieved, and it is a simple procedure [18,19,20]. However, temperature up-shift can activate physiological responses in *E. coli,* such as the heat shock response, stringent and SOS responses depending on the temperature increase and the time of the insult [18,19,20,21,22]. The heat shock response starts the expression of genes coding for proteins that provide structure and stability to nascent proteins such as chaperones and proteases [18,19,20,21,22]. Moreover, the production of RPs inducible by an increase in temperature can cause a negative effect on the biomass growth, increase the secretion of acetate, and cause different stresses related to heat shock, metabolic overload, and IBs formation [18,19,20,21,22,23].

Temperature is a parameter that affects RP production and aggregation [6,23,24,25,26,27]. Using other *E. coli* induction systems, temperature below 37°C favors the RP obtention in the soluble fraction, or the IBs formed could present biological activity since they could contain correctly structured protein [3,6,18,19,25], while 37°C or higher can promote the formation of aggregates, favoring intermolecular interactions with low native intramolecular contacts that decrease the correct folding of proteins inside the aggregates [18,19,24,25,28]. The RP production under thermoinducible systems commonly leads to IB formation [18,19,22], but the architecture and physicochemical characteristics of these IBs have been scarcely determined. Interestingly, in bioreactor cultures with an initial growth phase at 30°C and further thermoinduction at 39°C, the amount of IBs of SpA-galactosidase increased twice with respect to 42°C. However, at 42°C, the specific activity (U mg of cell dry weight^{-1}) of the SpA-galactosidase increased, showing important differences in IBs formation [28], while the comparison of the IBs formed in chemically induced systems and kept at 42°C or 37°C showed that IBs at 37°C are enriched with RP and present fewer host cell proteins than those obtained at 42°C [29]. Therefore, IBs produced at 37°C or above could have a lower proportion of well-structured protein than those formed at lower temperatures [24,30]. Moreover, IBs formed at 37°C or 42°C containing other RPs (G-CSF, GFP, His7dN6TNF-α) showed lower extractability in mild detergents compared with those formed at 25°C [25]. Thus, depending on the RP, temperature increases can affect the aggregation properties differently, as the IBs of asparaginase II produced at higher temperatures presented higher biological activity and less amyloid content [31]. Those observations suggest that optimizing temperature up-shift and other environmental parameters must be assessed protein by protein.

The human granulocyte and macrophage colony-stimulating factor (HuGM-CSF) has been produced recombinantly in *E. coli* in its non-glycosylated form, which has been used in the therapeutics of neutropenia and as an immunomodulator [32]. Typically, the industrial production bioprocesses of rHuGM-CSF contemplate the recovery of the recombinant protein from IBs, to later be denatured, refolded, and purified [33]. Recently, the recombinant form (rHuGM-CSF) has been used as a therapy in autoimmune pulmonary alveolar proteinosis [34] and is currently being tested in COVID-19 clinical trials [35]. The mature HuGM-CSF is composed of 127 amino acids with a theoretical molecular mass of 14.4 kDa and two disulfide bridges (Cys54-Cys96 and Cys88-Cys121) [36]. Despite the native protein-containing *O*- and *N*-glycosylation post-translational modifications, the rHuGM-CSF produced in *E. coli* which lacks these modifications has therapeutic effectivity [37].

The above highlights indicate that induction by temperature up-shift activates the RP overproduction and the heat shock response that can affect the productivity, associated with changes in metabolism and the content of RP in IBs [18,19,28]. However, the effect of thermoinduction on RP productivity and the IB architecture has been scarcely described [30,38,39]. Furthermore, the relationship between productivity and changes in structural IB characteristics has not been described at different temperatures of thermoinduction. Hence, we evaluated the kinetic thermoinduction effect (at 39°C and 42°C) in the growth and metabolism of a recombinant *E. coli* W3110 under λ*pL*/cI857 system as also on rHuGM-CSF productivity and especially on RP aggregation and the architecture of IBs.

2. Materials and methods

2.1. Strain, media, and cultivation conditions

E. coli W3110 (ATCC® 27325™) competent cells were transformed with plasmid pV3-uri200N (property of PROBIOMED S.A. de C.V.) encoding rHuGM-CSF (GeneBank accession number OL419360) under the promotor λ*pL* and expressing the cI857 repressor and the kanamycin resistance marker [40] constitutively. The rHuGM-CSF expressed was identified by Western Blot using the anti-hGM-CSF mouse antibody (MAB215 R&D Systems, Minneapolis, USA) and the antibody rabbit anti-mouse IgG-HRP (Zymed 61-6020). The Molgramostim European Pharmacopoeia (EP) Reference Standard was used as a control. Also, protein identification was performed in-gel digestion with trypsin or endoproteinase Glu-C and mass spectrometry [41]. The obtained peptides were extracted, concentrated, desalted, and analyzed by liquid chromatography in an Agilent nanoflow LC 1100 (Agilent, Waldbron Germany) coupled to mass spectrometry using a hybrid triple quadrupole and linear ion trap 3200 Q-TRAP (Applied Biosystems/MDS Sciex, Concord ON, Canada). The precursor ions were selected in Q1 with inspection spectra (enhanced mass spectra, EMS) following charge determination of the three main ions taking a high-resolution spectrum, and then for the fragmentation of such ions by collision active dissociation, using nitrogen in the collision cell Q2. The product ions were captured and analyzed in Q3 (enhanced product ion spectra). The MS/MS spectra interpretation was obtained with the Mascot program (https://www.matrixsicence.com).

One positive clone was used to elaborate the master and working cell banks containing 30% of glycerol in LB media and maintained at −70°C. Inoculum and cultures were grown in defined medium (MM) at pH 7.2 ± 0.2 [30,40], composed by (in g/L): $(NH_4)_2HPO_4$, 4.0; KH_2PO_4, 13.3; citric acid, 1.7; $MgSO_4{\cdot}7H_2O$, 1.2; thiamine hydrochloride, 0.045; kanamycin, 30 μg/mL; glucose,17.5; casamino acids, 3.0; and trace element solution, 2 mL. Concentrated solution (500X) of trace elements had the following composition (g/L): Fe-(III) 100.08, $ZnSO_4{\cdot}2H_2O$ 32.0, $MnCl_2{\cdot}4H_2O$ 15.0, H_3BO_3, 3.0, EDTA 14.1, $CoCl_2{\cdot}6H_2O$ 2.5, $Na_2MoO_4{\cdot}2H_2O$ 2.1, $CuCl_2$ 0.1. Glucose solution, $MgSO_4{\cdot}7H_2O$, and trace elements were sterilized separately from the culture medium. Thiamine, casamino acids, and kanamycin solutions were sterilized by filtration (0.22 μm membrane filter, Merck-Millipore, USA) and incorporated into the culture media [40].

Inoculum started with 1.0 mL of the working cell bank in a 250 mL Erlenmeyer flask with 50 mL of MM for 12 h at 30°C and 200 rpm (C-25, New Brunswick Scientific, USA). Bioreactors were inoculated with 10% of working volume with initial absorbance of ∼0.1 absorbance units (A.U.) for all cultures, which were performed by triplicate in a working volume of 0.8 L of media in a glass stirred bioreactor (1.2 L nominal volume) with two standard Rushton turbines, an L-type sparger and heating jacket (Applikon Biotechnology, Netherlands) [30,40]. The pH (AppliSens, Applikon Biotechnology, Netherlands) and dissolved oxygen tension (DOT, Mettler Toledo, USA) sensors were connected to ADI1010 Biocontroller (Applikon Biotechnology). DOT was calibrated for bubbling air (100%) and bubbling nitrogen (0%) when culture conditions were established (temperature, airflow, and stirrer speed). The Bioexpert Lite software (Applikon Biotechnology, Netherlands) was used to follow and acquire the online data [30,40].

Initial growth was controlled at 30°C, 400 rpm, and 0.8 standard air liters per minute. The temperature was increased to 39°C or 42°C to induce the RP production when the culture reached 3.0 absorbance units (A.U., around 7 h). DOT started near 100% and decreases according to bacterial metabolism, and during thermoinduction, DOT was controlled at 30% by agitation cascade (400–1000 rpm) by a proportional-integral-derivative strategy [30,40]. During all cultures, pH was controlled at 7.2 ± 0.2 by adding 2 N NaOH and 2 N HCl. Foaming was controlled by adding a silicone-based antifoam (New Brunswick 2097-87).

2.2. Analytical methods (cell concentration, glucose, and organic-acid quantification)

Bacterial growth was measured by optical density at 600 nm (OD_{600}) (Genesys 5 spectrophotometer, Thermo Fisher Scientific, USA) [30,40]. Cell absorbance was converted to dry cell weight using a linear correlation standard curve (1 A.U. = 0.35 ± 0.03 g/L). Biomass was harvested by centrifugation at 5,900 *g* at 4°C for 10 min (Eppendorf 5415C Centrifuge Hamburg, Germany). Glucose concentration was measured by the Biochemistry Analyzer YSI-2900 (YSI Life Sciences, USA) and corroborated in the Y15 automatized analyzer (Biosystems, Barcelona, Spain). Organic acids were analyzed by high-performance liquid chromatography (HPLC, Shimadzu, Japan) using an Aminex HPX-87H column (300 × 7.8 m m; 9 μm internal diameter, BioRad, USA) equipped with a UV detector. Supernatant samples were prefiltered (0.22 μm Minisart® Syringe Filters, Sartorius, Germany) and then separated with a mobile phase of 0.004 M H_2SO_4, with a constant flow rate of 0.6 mL/min at 50°C (LC Solutions v1.25 software Shimadzu, Japan). The separation of organic acid standard under the same conditions allowed for their quantification (Catalog No. 125-0586, BioRad, USA).

2.3. IB isolation

IBs were recovered from biomass pellet resuspended in lysis buffer (50 mM HCl-Tris 50, 1 mM EDTA, 100 mM NaCl, pH 7.5) with 1 mM of a protease inhibitor, PMSF (Merck-Sigma, USA). The cellular suspension was lysed by sonication (SoniPrep 150, Richmond Scientific, UK) at an amplitude of 8 μm in 6 steps of 30 s intervals, on ice [4,5], as an efficient method for cell disruption [42,43]. The cellular suspension was centrifuged at 10,000 *g* for 10 min at 4°C. The pellet fraction was agitated in the same buffer supplemented with 1.0% (v/v) of IGEPAL CO-630 (Merck-Sigma) for 30 min at 4°C and centrifuged at 10000 *g* for 10 min at 4°C. This second pellet enriched in IBs was resuspended in a buffer containing 0.5% (v/v) of Triton X-100 (Merck-Sigma, USA), agitated for 30 min, and centrifuged at 10000 *g* for 10 min at 4°C. The IBs were washed seven times with deionized low-conductivity water. The total protein was quantified from the lysed pellet fraction previously solubilized for 3 h in IEF buffer (7 M urea, 2 M thiourea, 2% CHAPS w/v, and 40 mM DTT) [44].

2.4. Total cellular protein and recombinant-protein quantification and identification

The Bradford assay was used to measure the protein concentration in 96-well microplates using Dye Reagent Concentrate following the manufacturer's recommendations (Bradford, 1976; Bio-Rad Protein Assay, USA). Total cellular protein, insoluble protein, and IBs were treated with IEF buffer for 3 h and diluted 5 times in water before quantification. Bovine serum albumin (GE Healthcare Bio-Sciences, MA, USA) was used as a standard. The samples were prepared in biological triplicates and technical duplicates.

The percentage of rHuGM-CSF in total protein was estimated in samples collected from three bioreactors, using densitometry analysis after separation by 12% SDS-PAGE stained with Coomassie Brilliant Blue R-250 (Bio-Rad, USA) with the Image Lab software on Gel Doc EZ System (Bio-Rad, USA) and corroborated by GelAna-

lyzer 19.1 software (https://www.gelanalyzer.com). We added 50 μg of protein per lane. The percentage of recovered rHuGM-CSF in IBs from three bioreactors was estimated by densitometry analysis in 15% SDS-PAGE stained with Coomassie Brilliant Blue R-250 (Bio-Rad, USA). IBs harvested at 1, 5, and 10 h post-induction were extracted at the same absorbance, and equal volumes were added to each well. The page ruler pre-stained protein ladder (Thermo Fisher Scientific, MA, USA) was used as a molecular weight marker. As a reference, we used rHuGM-CSF (Y0000251, Molgramostim CRS, European Pharmacopoeia Reference Standards).

2.5. Resistance to proteolytic digestion of isolated IBs

IBs harvested at 5 h and 10 h after induction were digested with 50 μg/mL of proteinase-K (PK, Sigma Aldrich, St. Louis, MO, USA) at room temperature, and the reaction was monitored for 30 min measuring OD at 350 nm (UV/Vis DU 730, Beckman Coulter, USA) mixing by pipetting every minute. The proteolytic digestion containing 200 μg/mL of purified IBs was resuspended in 50 mM Tris-HCl and 150 mM NaCl pH 8.0 buffer. The maximal absorbance was used for normalization [4,5]. Each analysis was carried out in biological triplicates.

Also, 50 μg/mL of IBs was digested for 30 min in the presence of 12.5 μg/mL of PK in 200 μL of 50 mM Tris-HCl, 150 mM NaCl pH 8.0 buffer. The reaction was centrifuged at 8,000 *g* for 5 min, and the supernatant was concentrated to 20 μL in a SpeedVac Concentrator Savant ISS110 (Thermo Fisher Scientific, USA). The reaction was loaded onto an SDS-PAGE 18% gel and silver-stained [45]. The quantification of the solubilized protein was performed by the Bradford method.

2.6. Attenuated Total Reflection-Fourier Transform Infrared (ATR-FTIR) spectroscopy of isolated IBs

IBs harvested at 3 h, 5 h, and 10 h were evaluated by ATR-FTIR spectroscopy to determine their secondary structure. IBs were previously dried in a SpeedVac Concentrator Savant ISS110 (Thermo Fisher Scientific, USA). Samples were analyzed on a Shimadzu IRAffinity-1S FTIR spectrophotometer (Shimadzu, Japan) with a Specac Quest ATR diamond accessory (Specac Limited, UK). At least 40 interferograms between 1500 and 1700 cm^{-1} was acquired using a 2 cm^{-1} resolution, registered, and averaged per sample after blank subtraction. Spectra data were subjected to the second derivative and smoothing with 13 points following the Savitzky-Golay method using IR Solutions software (Shimadzu, Japan). The bands corresponding to respective secondary structures were identified in the second derivative spectra [46,47] and were normalized to a tyrosine peak at ~1510 cm^{-1} [4]. Each analysis was carried out in biological triplicates and technical duplicates.

2.7. IB Thioflavin-T binding assays

Thioflavin-T (Th-T) binding assays were carried out to determine the amyloid content in IBs harvested at 5 h and 10 h after induction at 39°C and 42°C. A concentration of 70 μg/mL of IBs was resuspended in PBS pH 7.5 together with 75 μM of Th-T (Merck-Sigma-Aldrich) [4,40,48] and incubated for 30 min at room temperature. The excitation wavelength used was 445 nm, and emission spectra were recorded from 450 to 560 nm (Cary Eclipse fluorescence spectrophotometer, Agilent, USA). Apertures of the slits in the excitation and emission were set at 5 nm. Th-T (75 μM) in PBS was used as a control. A Gaussian distribution analysis of Th-T binding to IBs obtained in heat-induced cultures at 39°C and 42°C at different culture times was performed.

2.8. IBs in cells image analysis by Transmission Electron Microscopy (TEM)

The morphology and size of the IBs were analyzed using TEM. The protocol for fixing and staining the samples for TEM has been described by Castellanos-Mendoza et al. [5]. Briefly, samples of cells isolated at 1 h and 5 h post-induction were fixed for 4 h with 4% paraformaldehyde and 2.5% glutaraldehyde in sodium cacodylate buffer (0.16 M pH 7.4) at 4°C. Cell samples were post-fixed with 1% osmium tetraoxide for 90 min at 4°C and rinsed twice in chilled buffer and six times in cold distilled water, followed by dehydration in a series of ethanol solutions and then embedded in Epon. Thin sections were stained with uranyl acetate and lead citrate. A Libra 120 plus (Zeiss, USA) electron microscope was used. The percentage of cells containing IBs was estimated by observing at least 300 cells from different frames and obtaining their proportion with electrodense material. The maximal size of IBs within cells harvested after thermoinduction was also measured.

2.9. Solubilization of isolated IBs with guanidine hydrochloride

The purified IBs harvested at 5 h and 10 h after induction were solubilized using different concentrations of GnHCl (1, 2, and 4 M; Sigma-Aldrich) and 50 mM Tris-HCl buffer, 5 mM DTT, pH 7.5 during 24 h [5,40]. IBs at an initial concentration of 200 μg/mL were incubated. The content in the soluble fraction was determined by Bradford assay (Bio-Rad Protein Assay). Each analysis was carried out in biological triplicates and technical duplicates.

2.10. IB solubilization, refolding, and purification of rHuGM-CSF

About 300 μg of IBs was solubilized in IEF buffer and was separated on 18% of SDS-PAGE, and only a fraction of the gel was visualized by Coomassie blue staining. The rHuGM-CSF band was separated with a blade from the unstained gel, washed, and eluted at 4–8°C for 24 h in water [49]. Protein was refolded at 4–8°C by slow dilution (1:10) in Tris base buffer (20 mM, pH 8.2) and then concentrated in a 3-kDa cutoff Millipore Amicon concentrator [40].

The folded protein solution (~10 μg) was purified by reverse-phase HPLC (LC-20AT, Shimadzu, Kyoto, Japan) using a Zorbax Eclipse XDB-C8 column (Agilent Technologies, Santa Clara, CA, USA) at 50°C with a detector wavelength of 214 nm and a maximum column pressure of 3,000 psig [40]. The reference human GM-CSF (Molgramostim, Y0000251, Sigma Aldrich, St. Louis, MO, USA) was used as standard. Trifluoroacetic acid (TFA) in water (0.1% v/v) (mobile phase A) and 0.1% v/v TFA in 90% acetonitrile (mobile phase B) were used for the linear gradient elution, using a flow rate of 1.2 mL/min [40].

2.11. Circular dichroism (CD) spectroscopy

CD spectra were recorded at 37°C as previously reported [40]. The far-UV region was used in a JASCO J-720 spectropolarimeter (Jasco Inc., Easton, MD) [50]. In a quartz cell (0.1-cm length path), the refolded protein solutions (~0.05 mg/mL) were loaded. Each spectrum corresponds to the average of three repetitive scans corrected by the buffer signal. Ellipticities are reported as mean residue ellipticity, $[\theta]_{mrw}$. The secondary structure composition of rHuGM-CSF was calculated using the deconvolution software K2D3 [51].

2.12. Statistical analysis

Each condition was evaluated at least in triplicate. Independent samples and multiple-comparison tests were used to estimate significant differences in the culture parameters (two-way analysis of

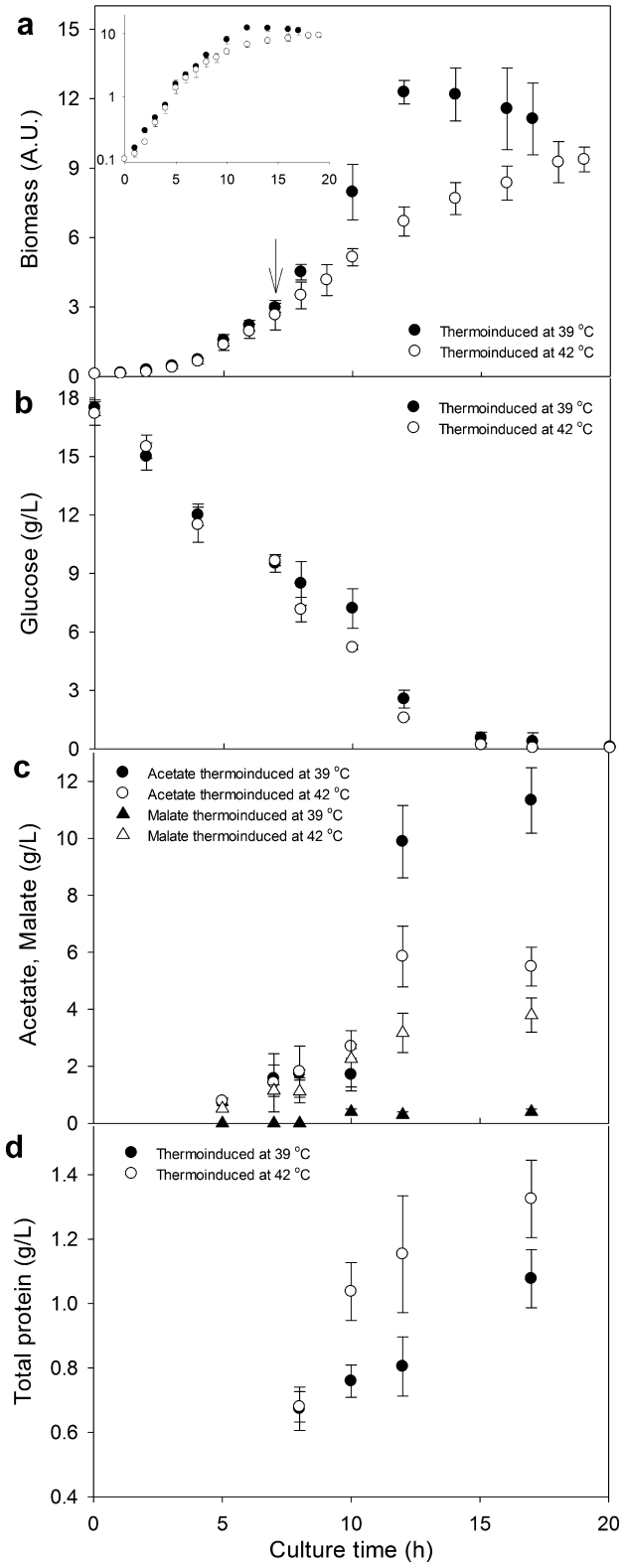

Fig. 1. Growth kinetics of *E. coli* W3110 expressing rHuGM-CSF thermoinduced at 39°C or at 42°C. Data show the average and standard deviation of the cultures carried out at least in triplicate. Temperature up-shift was performed when the culture reached 3.0 A.U. (around 7 h of culture). (**a**) Biomass growth (the inset presents the growth by a logarithmic axis). (**b**) Glucose consumption. (**c**) Total protein concentration. (**d**) Kinetics of acetate produced by *E. coli* W3110 in cultures induced at 39°C or 42°C, and malate at 39°C or 42°C. Data show the average and standard deviation of the cultures carried out at least in triplicate.

variance ANOVA and Tukey's posthoc test were used). A threshold significance level of 95% ($P < 0.05$) was applied.

3. Results

3.1. Identification of recombinant rHuGM-CSF

The rHuGM-CSF was identified by a specific Western Blot (Fig. S1) and by mass spectrometry. The obtained peptides from rHuGM-CSF digested in-gel with trypsin give two peptides, with a Mascot global score of 76 for HuGM-CSF, and the rHuGM-CSF digested in-gel with endoproteinase Glu-C obtained 51% of the total sequence of HuGM-CSF.

3.2. Differential thermoinduction affects recombinant E. coli W3110 growth

The growth kinetics of *E. coli* W3110 and the rHuGM-CSF production were analyzed using two induction temperature up-shifts (from 30°C to 39°C and 30°C to 42°C). Before induction, cell growth at 30°C was identical for both conditions (Fig. 1A, Table 1). After induction, the culture with a temperature up-shift to 39°C reached almost twice biomass after 12 h of culture compared with the culture induced at 42°C (Fig. 1A, Table 1). The post-induction specific growth rate (μ) was ~25% higher in the cultures induced at 39°C with respect to those induced at 42°C (Table 1). The μ after temperature up-shift was 0.28 ± 0.02 h^{-1} and 0.22 ± 0.02 h^{-1} for 39°C and 42°C, respectively (Table 1). Despite the differences in maximum biomass concentration, it is interesting to note that the glucose consumption in both cultures was similar during the full cultivation course (Fig. 1B). However, there was a 23% higher yield of biomass/glucose ($Y_{X/S}$), and a 20% higher specific glucose consumption rate (q_s) at 39°C in comparison with that observed at 42°C (Table 1).

Table1
Stoichiometric and kinetic growth parameters of *E. coli* W3110 growing at two post-induction temperatures and its production of rHuGM-CSF.

Parameter	Temperature post-induction	
	39°C	42°C
μ pre-induction (h^{-1})	0.48 ± 0.05	
[A]μ post-induction (h^{-1})	0.28 ± 0.02[a]	0.22 ± 0.02[b]
X_{max} (g/L)	5.52 ± 0.22[a]	4.21 ± 0.23[b]
[B]$Y_{x/s}$ (g/g)	0.31 ± 0.01[a]	0.24 ± 0.01[b]
[C]Acetate (g/L)	11.33 ± 1.15[a]	5.85 ± 1.06[b]
[D]Malate (g/L)	0.40 ± 0.09[a]	3.80 ± 0.60[b]
[E]Total protein (g/L)	1.08 ± 0.09[a]	1.32 ± 0.12[b]
[F]$Y_{P/X}$ (g/g)	0.21 ± 0.02[a]	0.32 ± 0.04[b]
[G]rHuGM-CSF in IB (%)	28 ± 5[a]	43 ± 5[b]
[H]rHuGM-CSF in total protein (%)	29 ± 2[a]	37 ± 2[b]
[I]rHuGM-CSF (g/L)	0.31 ± 0.02[a]	0.49 ± 0.03[b]
[J]q_s (g/g*h)	0.33 ± 0.03[a]	0.27 ± 0.02[b]

The values represent the mean and standard deviation for three biological replicates per condition. The statistical differences are indicated with different letters ($p < 0.05$).
A: specific growth rate post-induction was calculated from the slope of growth after induction and before the stationary state.
B: $Y_{x/s}$ was calculated from glucose consumption until the X_{max} in each condition.
C, D, E, F, H: Acetate, malate, total protein, and $Y_{p/x}$ were calculated at maximum values.
G, H: rHuGM-CSF percentage in IBs was based on densitometric analysis from bands identified in SDS-PAGE gels (Fig. 2).
I: rHuGM-CSF (g/L) was calculated by multiplying Total protein (g/L) × rHuGM-CSF in total protein (%).
J: specific glucose consumption rate was calculated after induction (once cultures reached ~3 A.U. until the glucose exhaustion).

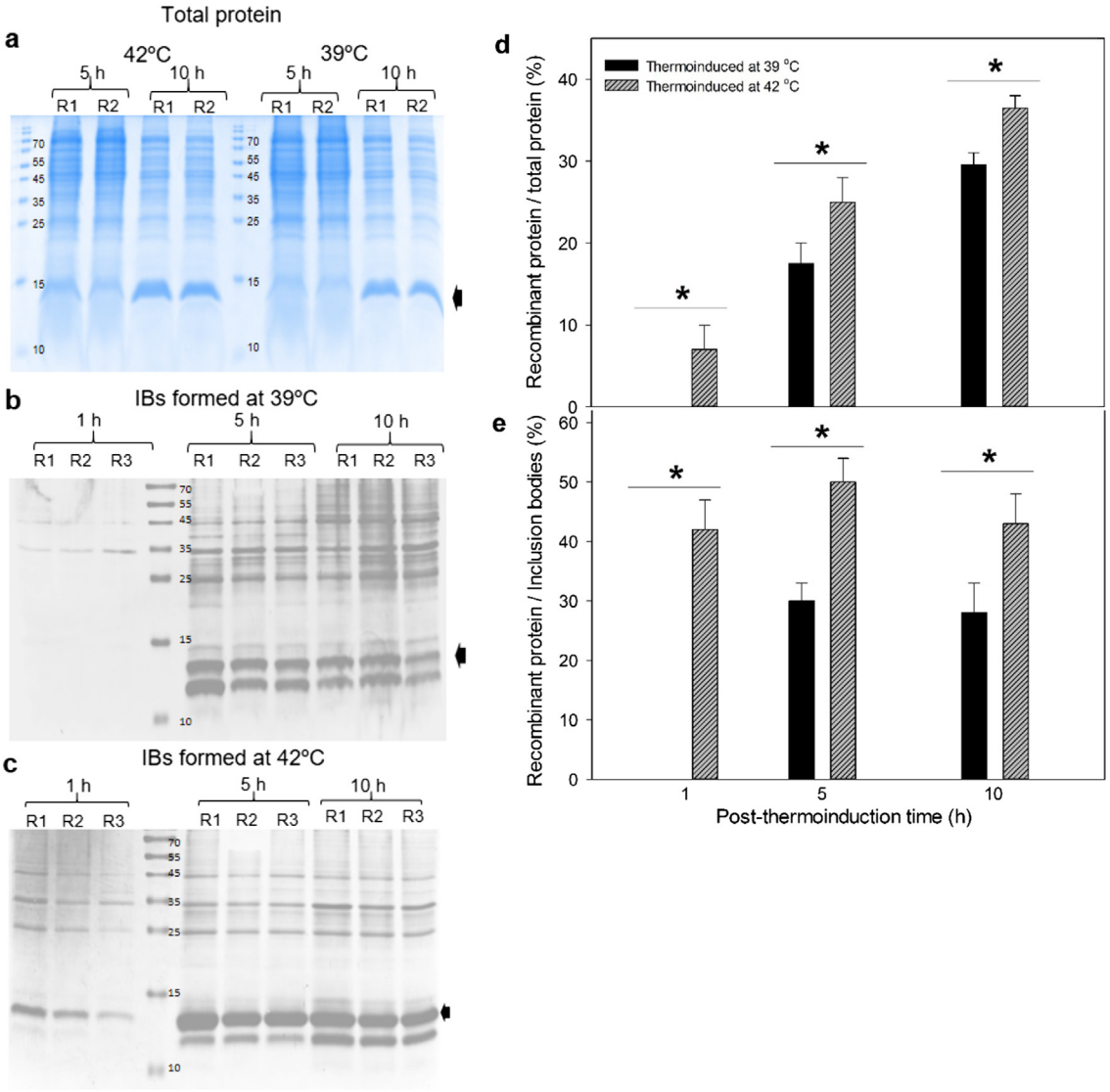

Fig. 2. Accumulation of rHuGM-CSF at two induction temperatures. (**a**) SDS-PAGE profiles of total protein of *E. coli* producing rHuGM-CSF at different induction temperatures in SDS-PAGE at 5 and 10 h. Lane M, molecular weight marker (kDa). (**b**) and (**c**) Distribution of rHuGM-CSF accumulated into inclusion bodies fraction in cultures thermoinduced at 39°C and 42°C, respectively (R1, R2, and R3: samples taken in cultures in bioreactors one, two and three, respectively). The arrow indicates the expression of rHuGM-CSF. The comparison of the rHuGM-CSF with the international standard (molgramostim) is presented in Fig. S1 and Fig. S2. (**d**) Time-course comparison of rHuGM-CSF / total protein and (**e**) time-course kinetic comparison of rHuGM-CSF / IBs in cultures thermoinduced at 39°C and 42°C, respectively. In (**d**) and (**e**), data show the average and standard deviation of the cultures carried out in triplicate.

3.3. Effect of thermoinduction on organic acid accumulation

Acetate is considered an undesirable by-product in aerobic *E. coli* cultures when glucose is used as a carbon source [52]. Typically, acetate accumulation affects the RP yields and inhibits growth depending on the strain; in the case of a growth inhibition could occur between 7 and 13 g/L of acetate [52]. Although *E. coli* W3110 can grow in acetate under certain conditions through the glyoxylate by-pass [52,53]. The acetate accumulation was observed at the end of the growth phase (after 12 h), with the highest concentration obtained at 39°C (11.33 ± 1.15 g/L), while the cultures induced at 42°C accumulated half of the concentration (5.85 ± 1. 06 g/L, Fig. 1C, Table 1). Malate accumulation has been observed in aerobic *E. coli* cultures under heat shock, possibly associated with the up-regulation in genes coding for TCA enzymes [54]. Here, malate accumulated reaching concentrations of 4 g/L in cultures at 42°C, while at 39°C, it was maintained lower than 1 g/L (Fig. 1D, Table 1). Succinate, oxalate, and citrate were not detected in any culture.

3.4. Effect of thermoinduction on total protein and rHuGM-CSF accumulation

In *E. coli*, temperature up-shift above 37°C causes heat stress, metabolism changes, resource distribution to restore homeostasis, and a decrease in biomass synthesis [18,19]. Furthermore, the expression levels of genes involved in metabolism change continuously when heat stress is applied steadily [54]. As a rearrangement of metabolism happens, it is feasible to assume that the intracellular conditions change modifying the RP accumulation and aggregation [18,19]. Cultures induced at 42°C reached 20% more total protein compared with those induced at 39°C (Fig. 1D, Table 1). This indicates that induction at 39°C did not unbalance cell homeostasis, favoring biomass accumulation without affecting the total protein synthesis. At 42°C, the biomass synthesis was reduced, and the total protein synthesis was favored. Comparing the protein yield over biomass ($Y_{P/X}$), a 1.5-fold improvement in the protein synthesis per cell cultured at 42°C is evidenced (Table 1).

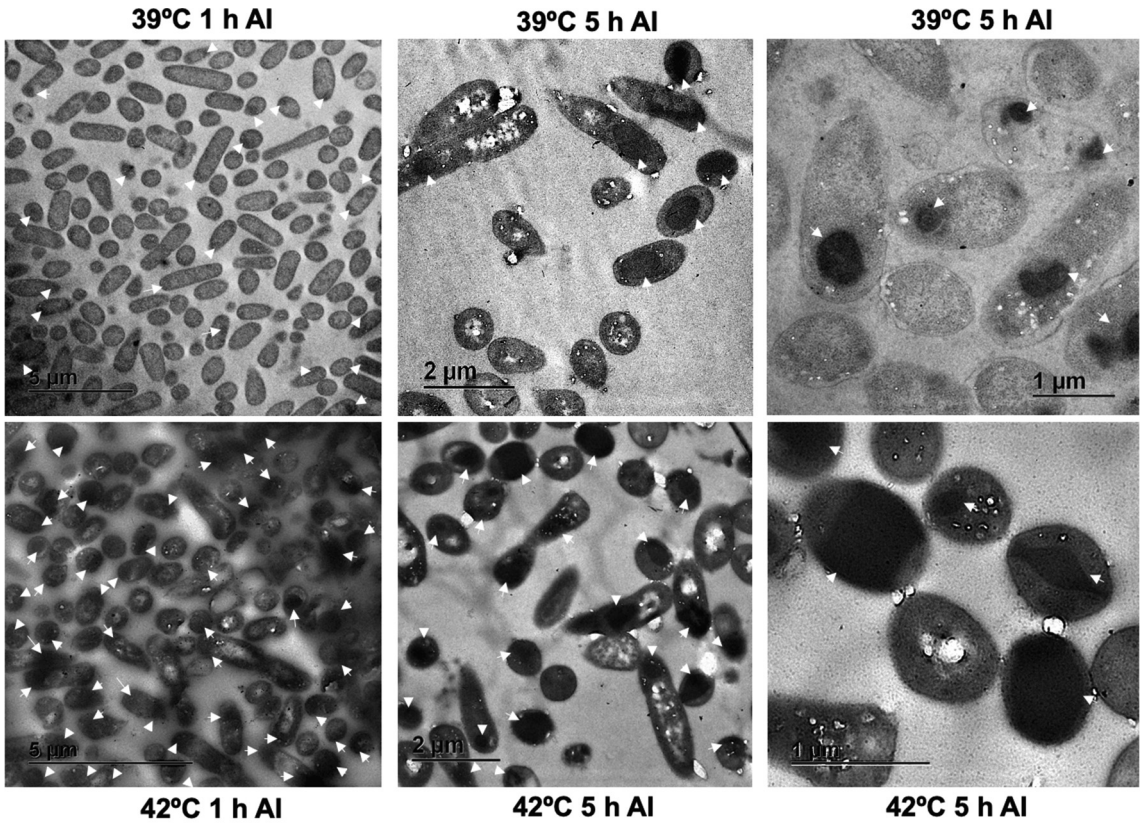

Fig. 3. Micrographs of cross-sections of *E. coli* W3110 producing rHuGM-CSF viewed under the transmission electron microscope (TEM) and harvested after 1 or 5 h of thermoinduction at 39°C (upper images) or 42°C (bottom images). **Left:** cells harvested after 1 h of thermoinduction (scale bars 5.0 µm). **Center:** cells collected after 5 h of thermoinduction (scale bars 2.0 µm). **Right:** cells harvested after 5 h of thermoinduction (scale bars 1.0 µm). Inclusion bodies are electrodense particles indicated by white arrows. Scale bars represent the size indicated in each micrograph.

The rHuGM-CSF produced in *E. coli* W3110 cultures was evaluated at 1 h, 5 h, and 10 h after thermoinduction. The rHuGM-CSF accumulated over time under both induction temperatures (Fig. 2A, 2D). After 1 h, 5 h, and 10 h of cultivation at 42°C, there was ~8% more accumulated RP per total protein compared to the culture up-shift at 39°C (Fig. 2A, 2D, Table 1). The percentage of the rHuGM-CSF present in IBs was determined by densitometry of the SDS-PAGE from three independent cultures at 1 h, 5 h, and 10 h after thermoinduction (Fig. 2B, 2C, 2E, Fig. S2). In the cultures induced at 42°C, the RP in IBs obtained 1 h after thermoinduction was significantly higher than 39°C (Fig. 2B, 2E). This implies variations in protein synthesis that could be important for the formation of the IBs. At the end of the culture, the percentage of rHuGM-CSF with respect to the content of endogenous protein in IBs was lower in the cultures induced at 39°C compared to those induced at 42°C (Fig. 2E). Although a similar host cell protein banding pattern is seen in IBs at 5 h and 10 h after thermoinduction (Fig. 2AA, 2B, and 2C), the intensity and proportion of each one is different when comparing both conditions.

3.5. Induction temperature modified the onset of IB formation

Cell morphology was analyzed after 1 h and 5 h of thermoinduction under Transmission Electron Microscopy (TEM) (Fig. 3). IB shape and size can be modified by cultivation time, pH changes, and agitation among others [4,5,6,55]. IBs are observed in TEM as electrodense protein clusters with semispherical, spherical, or cylindrical shapes [6]. The induction temperature affected the initial IB formation time (Fig. 3), although no significant differences in shape or size were observed after 5 h of thermoinduction. The size of IBs inside the cells was around 600 to 800 nm. Examining at least 300 cells, the percentage of cells in which IBs can be seen is greater in cultures thermoinduced at 42°C than those at 39°C. At 1 h after induction at 39°C, only 12% of cells include IBs, while at 42°C, 40% of cells contain IBs (Fig. 3). At 5 h post-induction and 39°C, almost 32% of cells contained IBs but at 42°C, 63% of the entire culture presented IBs.

3.6. Resistance of IBs to proteinase-K degradation

The kinetics of proteolytic degradation by PK was studied to understand the effect of induction temperature on the aggregation of IBs [4,5,48,55]. PK digestion analysis identifies differences in loops and α-helical domains with hydrophilic characteristics easily cleaved, in comparison with regions inside β-sheet which are partially resistant to proteolysis [5,48]. All experiments started with the same protein content (200 µg/mL), and a normalization of the absorbance was done. The kinetics of IB sensitivity to proteolysis was measured as the decrease in turbidity at 350 nm upon the addition of PK. It is assumed that when measuring at 350 nm, the aggregated protein contributes to the turbidity and when part of the IBs is solubilized, this soluble state does not contribute to the absorbance [24]. The IBs formed at 39°C and 42°C and harvested after 5 h and 10 h of thermoinduction were degraded similarly (Fig. 4A, 4B). The first 5 min data could be fitted to a second-order equation and the differences in the apparent rate constants of the fast phase were calculated. Comparing induction temperatures, the degradation rate of IBs by PK (in the first 5 min of the test) was statistically similar at the same harvest time. Importantly at the end of the PK reaction time, the IBs formed at 39°C were less

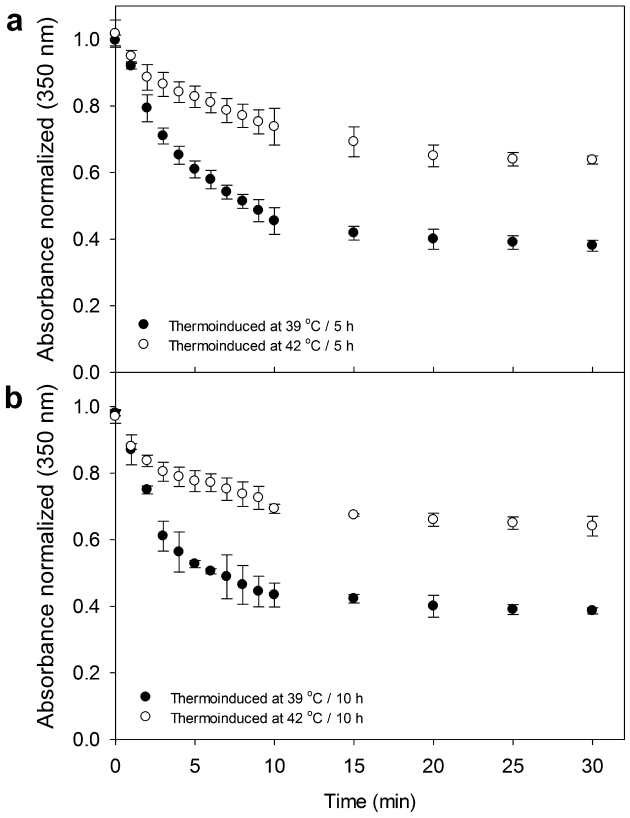

Fig. 4. Proteolysis time course of rHuGM-CSF IBs harvested at 5 h (**a**) and 10 h (**b**) after thermoinduction at 39°C or 42°C with proteinase-K (PK). The degradation was followed by absorbance and data were normalized. Data show the average of triplicate experiments from three independent bioreactors each.

resistant to proteolysis reaching a degradation of around 60%, while those IBs formed in cultures induced at 42°C only were degraded by 35%, despite having similar sizes. This indicates that the IBs formed at 39°C are different in protein composition and internal structure compared with those formed at 42°C (Fig. 4A, 4B). When 50 μg/mL of IBs was digested in the presence of 12.5 μg/mL, PK treatment releases almost twice the protein from IBs formed at 39°C (18.0 ± 2.2 μg/mL) with respect to those formed at 42°C (9.5 ± 2.1 μg/mL) measured by the Bradford method and corroborated by silver-stained SDS-PAGE (Fig. S3).

3.7. Secondary structure of thermoinduced IBs by ATR-FTIR

We determine the effect of the induction temperature on the elements of the secondary structure within the IBs formed at 39°C and 42°C by ATR-FTIR. The major bands were identified, and respective secondary structures were assigned (Fig. 5). To establish differences in structural composition, data were analyzed for the main secondary structures based on the distribution previously assigned [31,46,47]. The bands in the region near 1652 ± 5 cm^{-1} were assigned as α-helices, and bands close to 1630 ± 4 cm^{-1} were assigned as β-structure [31,47]. The bands in region 1622–1626 cm^{-1} were assigned as intermolecular β-structures that can be related to the formation of aggregates and mostly to their amyloid conformation [56,57].

We analyzed the effect of both induction temperatures on the IBs harvested at 3 h, 5 h, and 10 h after thermoinduction by biological triplicate. In the first 3 h of thermoinduction, significant differences can be observed in the α-helical content and in the presence of the amyloid-like conformation associated with the 1655 cm^{-1} and 1626 cm^{-1} bands, respectively (Fig. 5A, 5D). These bands increased in the IBs formed at 39°C compared with those obtained at 42°C. Data suggest that IBs formed at 39°C show a higher "amyloid-like" structure with respect to the time, and in comparison, with those formed at 42°C (Fig. 5D, 5E, and 5F), while α-helices and β-structure did not change after 5 h of thermoinduction.

3.8. IBs from thermoinduced cultures at 42°C bind less Th-T

Binding to Th-T was measured to determine modifications in the amyloid content of the IBs formed in the different induction temperatures. The dye Th-T exhibits a maximal fluorescence at 485 nm when it binds to the β-sheet surface of structured channels, without binding to monomers or amorphous structures [58]. Based on the Gaussian distribution fitting curve, the maximal emission for rHuGM-CSF IBs binding to Th-T was between 486 and 493 nm (Fig. 6, Table S1). The highest fluorescence signal was observed for the IBs produced under the thermoinduction of 39°C compared with those IBs formed at 42°C (Fig. 6A). A ratio of 2.4 times more Th-T binding to IBs is seen in those from cultures induced at 39°C than those at 42°C when the first parameter of the Gaussian equation is compared (Table S1). Results suggested a higher presence of cross-β structures in IBs formed at 39°C compared with those at 42°C, in agreement with the FTIR results (Fig. 5, Fig. 6).

3.9. Solubilization of IBs in guanidinium chloride (GnHCl)

In bioprocesses, the purification of RPs begins with the solubilization of the IBs [59,60]. Hence, we compared the solubilization of IBs obtained at 3 h, 5 h, and 10 h after thermoinduction at 39°C and 42°C using 0 M, 1 M, 2 M, and 4 M of GnHCl (Fig. 7). It was observed that those IBs obtained from cultures thermoinduced at 39°C are easier to solubilize compared to those formed at 42°C at all GnHCl concentrations evaluated irrespective of the time. At 4 M of GnHCl, almost a complete denaturalization for the IBs harvested at 3 h and 5 h in cultures thermoinduced at 39°C was observed, in contrast with the 80% of the protein solubilized from those IBs collected from thermoinduction at 42°C (Fig. 7A and 7B). However, the IBs recovered after 10 h of thermoinduction at both temperatures cannot be solubilized by the chaotropic agent to the same extent as those harvested at earlier times (Fig. 7C), although the greater solubility of the IBs formed under the thermoinduction of 39°C is maintained.

3.10. Refolding capacity of rHuGM-CSF from IBs

The refolding capacity of recovered rHuGM-CSF from IBs was characterized by far-UV CD spectroscopy, a technique sensitive to protein secondary structure content. The purified samples from IBs of the two thermal induction regimes showed similar spectra, typical of predominantly helical structures (Fig. 8). A deconvolution analysis of the CD spectra yielded α-helix and β-strand contents of 35% and 21% for rHuGM-CSF refolded from IBs formed at 39°C, and 36% and 15% for the protein at 42°C, respectively, which agree with those observed in the crystallographic structure of HuGM-CSF [36] and with rHuGM-CSF obtained with a thermoinduced system under different pre-incubation temperatures [40].

4. Discussion

This study showed that the induction temperature is a determining environmental factor in the production of RP and the structure of the IBs in thermoinducible systems. Previous reviews about

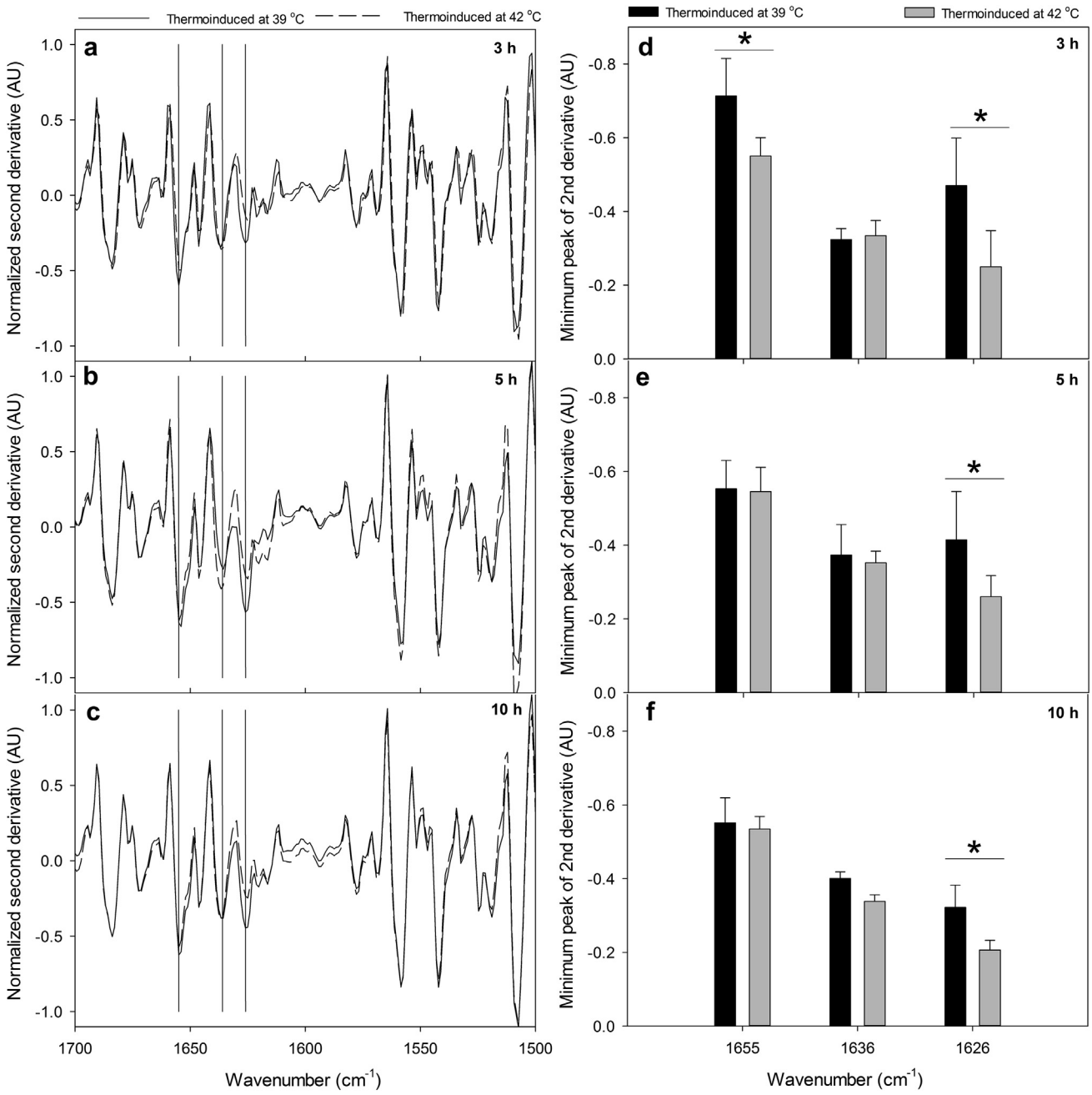

Fig. 5. Typical structural analysis of rHuGM-CSF IBs from cultures thermoinduced at 39°C or 42°C, after (**a**) 3 h, (**b**) 5 h and (**c**) 10 h by ATR-FTIR. The absorbance of the second derivative spectra was normalized against the tyrosine peak at ~1515 cm. The component bands employed to assign α-helix (~1655 cm^{-1}), β-sheet (~1636 cm^{-1}), and amyloid-like aggregation (~1626 cm^{-1}) are pointed out with vertical lines. Minimum height comparison of peaks of rHuGM-CSF IBs harvested at 39°C and 42°C indicates the main component bands obtained after (**d**) 3 h, (**e**) 5 h and (**f**) 10 h of thermoinduction. In (**d**), (**e**), and (**f**), data show the average and standard deviation of the cultures carried out in triplicate.

the production of RPs under thermoinduction conditions have discussed the advantages of high productivity in this regulable, simple to operate, and scalable system [18,19,22]. Numerous proteins have been produced under the λ*pL*/*pR*-cI857 system, using diverse configurations. The widest used strategy to promote biomass production consists of growing cells at 30°C followed by an increase to 42°C to induce the recombinant gene expression [20,40,61,62]. Furthermore, studies suggest that IBs are formed by different folding intermediaries of RP [6,25] being the temperature a parameter that can promote their aggregation [24,28,63]. However, to our knowledge, no work had addressed the importance of small differences in the induction temperature in the λ*pL*/*pR*-cI857 system on RP production, aggregation, and IBs architecture.

It was observed that during thermoinduction, the μ is negatively affected, because of the 'metabolic burden', where nutrients and energy are adjusted to synthesize RPs instead of biomass [18,19]. In this study, cultures thermoinduced at 39°C reached twice more biomass after 12 h of cultivation (~5 h of thermoinduction), compared to cultures grown at 42°C. Correspondingly, the higher biomass production was accompanied by an increase in the formation of acetate (Fig. 1) because of the unbalanced carbon metabolism, being a signal of metabolic overflow that can affect

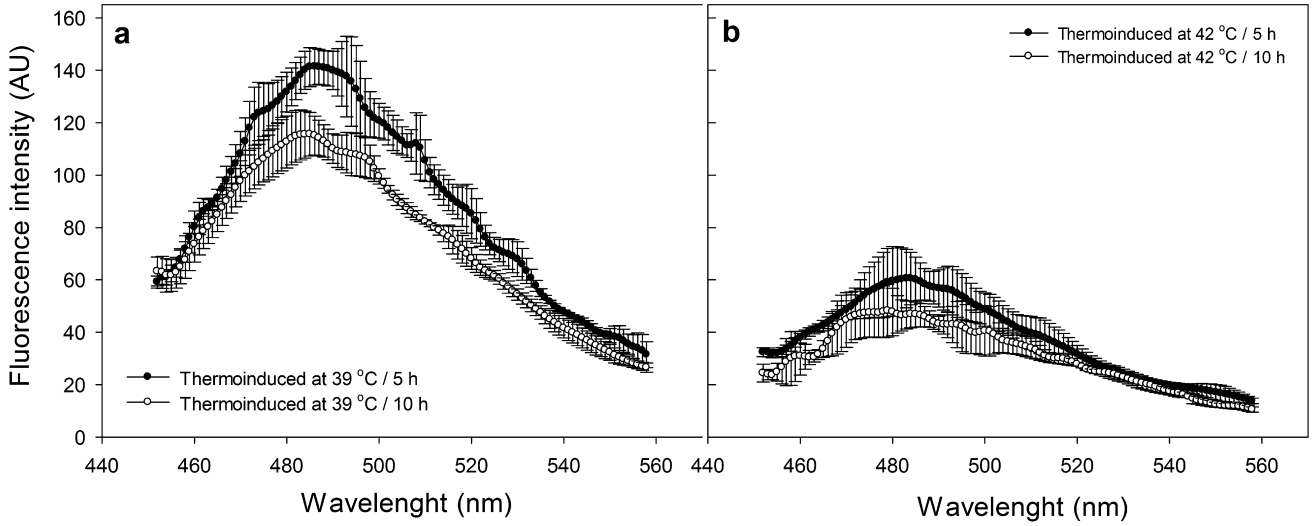

Fig. 6. Fluorescence of Th-T binding to rHuGM-CSF IBs collected at 5 h and 10 h after thermoinduction at 39°C (**a**) and 42°C (**b**). The maximal emission of rHuGM-CSF IBs binding to Th-T was between 486 and 493 nm. Data show the average of triplicate experiments from three independent bioreactors each using the same amount of protein quantified by Bradford.

the RP production [64]. Importantly, in the cultures induced at 42°C, the highest amount of total protein and RP was obtained, compared to the induction at 39°C (Fig. 1D). In addition, the enrichment of RP on total protein fraction and inside IBs increased with the culture time under both temperatures (Fig. 2), being higher at 42°C. The increase in production of total protein is possibly caused by a decrease in specific growth rate and low biomass formation (Table 1), lower production of acetate, and the use of building blocks to produce proteins and enhancement of translation [18,19].

IB formation can be due to hydrophobic interactions between protein chains, the elevated local concentration of proteins emerging on nearby ribosomes, and the diminished availability of chaperones [65]. Thermoinduction may improve protein synthesis exposing a greater number of hydrophobic regions and elevating the probability of interaction, and the formation of aggregates. The protein composition of IBs formed at 39°C and 42°C was different (Fig. 2). The IBs formed at 42°C were enriched with rHuGM-CSF (Fig. 2). Fig. 2E shows the percentage representation of the rHuGM-CSF inside IBs, considering each lane independently. The IBs formed at 42°C contained around ~40% of rHuGM-CSF after the first hour of induction, while in the IBs formed at 39°C at the same time, the rHuGM-CSF was not detected (Fig. 2E). As observed in Fig. 2B and 2C, the rHuGM-CSF accumulation was enriched in the IBs formed at 39°C and 42°C, with respect to the time. Furthermore, the increment in the percentage representation of rHuGM-CSF inside IBs formed at 42°C was statistically higher compared to the percentage of the RP in IBs formed at 39°C. In the cultures induced at 39°C, the IBs presented a greater accumulation of proteins attached with molecular weights greater than 25 KDa (Fig. 2B, 2C). The differences found in rHuGM-CSF / total protein and rHuGM-CSF / IB ratios (Fig. 2D and 2E) with respect to time demonstrate differences in rHuGM-CSF production and aggregation kinetics.

Our results reveal formation details of the IBs composed of rHuGM-CSF formed at different temperatures. At the first hour of induction in thermoinduced cultures at 39°C, few cells with IBs were observed (~12%), while in cells thermoinduced at 42°C, IBs were evident (~40%) (Fig. 3). It is important to mention that the IBs formed at 39°C and 42°C after 5 h presented similar sizes of around 700 nm and semispherical shapes, without appreciating differences in intracellular arrangement (Fig. 3).

Reported data show that a decrease in temperature can favor the formation of IBs with biological activity such as fluorescence or enzymatic activity, since they consist of native-like conformations, possibly favored by the decrease in the synthesis rate [25]. However, in thermoinduced systems, a temperature up-shift is necessary to obtain RPs, which favors disorderly aggregation with less chance of reaching native-like conformations. Hence, studying the effect of different induction temperatures on IB architecture is essential to improve up- and down-stream steps of bioprocesses. IBs produced under thermoinduction suggest differences in susceptibility to digestion with PK, being those formed at 39°C prone to digestion in comparison with the IBs structured at 42°C (Fig. 4, Fig. S3). Also, a greater amount of protein was solubilized in IBs formed at 39°C, when using the chaotropic agent guanidinium chloride (Fig. 7). The contribution of the solubility using mild chaotropic agent concentrations (2 M or 4 M) favors the rHuGM-CSF recuperation from IBs formed at 39°C. This even, at the cost of losing the productivity of the RP, that is higher at 42°C, but avoiding extensive downstream steps [59].

Protein folding is a complex process, and even more when a variety of RPs and host cell proteins with a diversity of structures interact and are kept together inside the IBs [6,15,18,24,30]. IBs consist of unfolded, partially folded, and even native structures of proteins trapped in a complex network, with some capable of acquiring an amyloid-like structure. The highest degradation of IBs formed at 39°C by PK indicates that they present a higher amount of exposed hydrophilic domains such as loops and α-helical structures rich in peptide bonds of aliphatic and aromatic amino acids in comparison with IBs from 42°C [5] corroborated by the higher amount of proteins and peptides liberated at 39°C compared with 42°C (Fig. S3). Since guanidinium chloride disrupts the hydrophobic and van der Waals interactions in proteins [66], results suggest that the hydrophobic domains are more accessible to the chaotropic agent in IBs formed in thermoinduction at 39°C and to a lesser extent (~20%) in the IBs produced at 42°C (Fig. 7).

The human GM-CSF is a glycoprotein formed by four short chains of α-helices, as well as, by one short antiparallel β-structure (PDB number: 2GMF). To analyze the architecture of the IBs, ATR-FTIR spectroscopy and Th-T dye-binding were used. The IBs produced at 42°C have a higher RP content, and a smaller concentration of endogenous proteins than those IBs formed at 39°C (Fig. 2). Interestingly, the IBs formed at 42°C presented lower

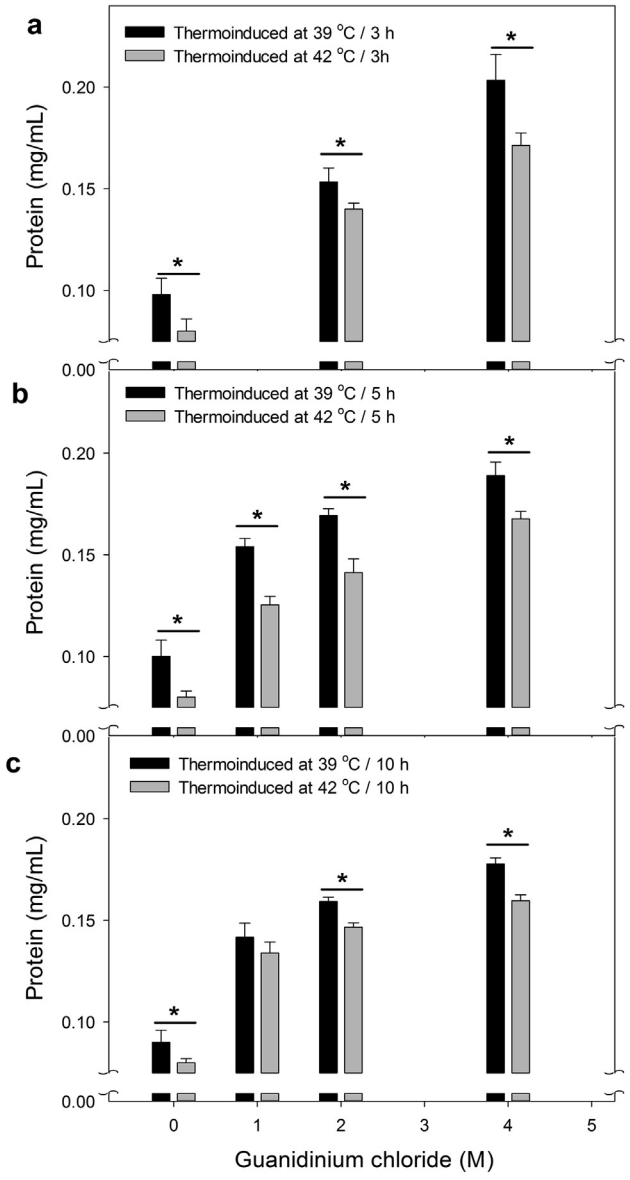

Fig. 7. Comparison of protein solubilization of rHuGM-CSF IBs collected at (**a**) 3 h, (**b**) 5 h, and (**c**) 10 h after thermoinduction at 39°C and 42°C, using different concentrations of guanidinium chloride. Data show the average of triplicate experiments from three independent bioreactors each.

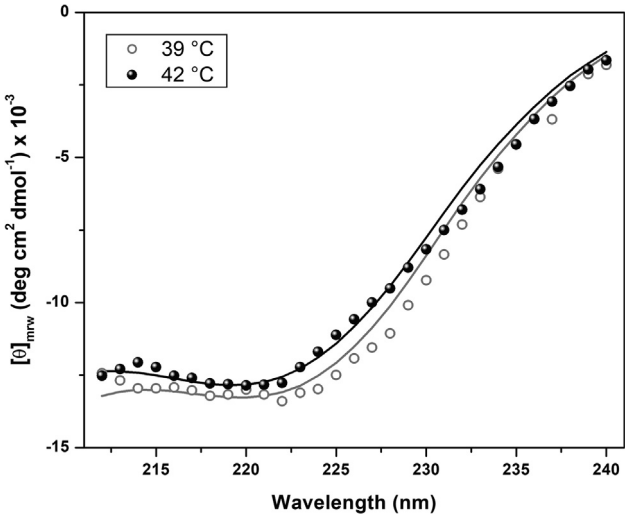

Fig. 8. Far-UV circular dichroism spectra of purified rHuGM-CSF in water from IBs obtained from thermoinduced cultures at 39°C or 42°C. Each spectrum corresponded to the average of three repetitive scans and was corrected by the buffer signal. The solid lines correspond to the mean residue ellipticity fits using the deconvolution K2D3 software [51].

amyloid-like structures than those formed at 39°C (Fig. 5). The comparison of the percentage of amyloid structure with respect to the total structures (α-helix, β-strands, and amyloid) resulted in a greater proportion in those IBs from cultures induced at 39°C (25–30%) with respect to those induced at 42°C (18–22%). This observation agreed with the results obtained by the Th-T binding assay (Fig. 6). A linear correlation (R^2 = 0.94) was found between the harvest points and the data obtained for the amyloid-like aggregation (~1626 cm^{-1}) by ATR-FTIR and cross β-structures measured as fluorescence intensity by Th-T binding (Fig. S4). Furthermore, the data obtained from ATR-FTIR suggested a reduced content of amyloid type in the IBs produced under thermoinduction at 42°C, like data found in IBs of recombinant asparaginase II produced in *E. coli* grown in orbital shake flasks, at 42°C and induced by IPTG [31].

We found that IBs formed at 39°C and 42°C initiated their structuration under different amounts of synthesized RP, being slower at 39°C, consistent with the lower amount of RP produced. These differences could cause distinct relations between RP and host cell proteins that could impact the conformers reached. Although IBs formed at 39°C have more amyloid structures, they are more soluble in a chaotropic agent and easily digested with PK, than those IBs formed at 42°C. This suggests a greater disorder in IBs formed at 42°C than those formed at 39°C, where the increase in protein concentration and inter-specific interactions relapse in rapid aggregation, without being able to acquire ultrastructure, as is the case of amyloid structures that can be formed with low protein concentration produced at 39°C. Hence, the high concentration of RPs produced in the bacterial cytoplasm could cause the differences observed. At the beginning of IBs formation in thermoinduced cultures at 39°C, the RP concentration is lower than those from 42°C, and endogenous proteins in high concentration might be added to the IBs, which can dictate the formation of the ultrastructure. While at 42°C, the formation of IBs is faster with higher RP concentration governing disordered aggregation, acquiring fewer amyloid forms, and being more resistant to degradation. This correlates with the amorphous aggregates formed at a high concentration of β2-microglobulin *in vitro*, which presented a fewer amyloid structure [65].

5. Conclusions

This study revealed that induction temperature determines *E. coli* growth, RP synthesis, its concentration, and protein aggregation, which impacts IB composition, architecture, and solubility in the thermoinducible system λ*pL*-cI857, using the rHuGM-CSF as a model RP. Thermoinduction *per se* favors the IB formation through the RP overproduction. However, slight differences such as three degrees (39°C *vs* 42°C) can cause differences in metabolism that favor either biomass synthesis at 39°C, while raising the temperature to 42°C limits biomass growth and favors the rHuGM-CSF production. These effects cause changes in protein production and the initiation of nucleation, aggregation, and IB formation.

Differential characteristics in IB architecture were also observed. IBs formed at 42°C were less prone to degradation and presented less amyloid-like structures, related to a rapid IB formation. In comparison, IBs formed slowly at 39°C presented a higher proportion of amyloid-like structures, being more susceptible to

degradation. In both thermoinduction scenarios, IBs were more resistant as the induction time increased. Altogether, the information described will allow the strategic design of thermoinduction to obtain a greater amount of RPs that can be extractable from the IBs. Information can be helpful to develop an improved bioprocess to produce therapeutic RPs in thermoinducible systems and to design rational protein recovery and purification strategies since the architecture of IBs is a determining factor to start the downstream bioprocess.

Authors contribution

- Study conception and design: S Restrepo-Pineda; E García-H ernández; NO Pérez; MA Trujillo-Roldán; NA Valdez-Cruz.
- Data collection: S Restrepo-Pineda; D Rosiles-Becerril; AB Vargas-Castillo; LP Ávila-Barrientos; A Luviano; NA Valdez-Cruz.
- Analysis and interpretation of results: S Restrepo-Pineda; LP Ávila-Barrientos; A Luviano; N Sánchez-Puig; E García-Hernández; NO Pérez; MA Trujillo-Roldán; NA Valdez-Cruz
- Draft manuscript preparation: S Restrepo-Pineda; MA Trujillo-Roldán; NA Valdez-Cruz
- Revision of the results and approved the final version of the manuscript: S Restrepo-Pineda; D Rosiles-Becerril; AB Vargas-Castillo; LP Ávila-Barrientos; A Luviano; N Sánchez-Puig; E García-Hernández; NO Pérez; MA Trujillo-Roldán; NA Valdez-Cruz

Financial support

Sara Restrepo-Pineda is a doctoral student from "Programa de Doctorado en Ciencias Biológicas", of the "Universidad Nacional Autónoma de México" (UNAM) and received a fellowship from CONACYT (CVU 589949). Axel Luviano; Nuria Sánchez-Puig; Enrique García–Hernández; Nestor O. Pérez; Mauricio A. Trujillo-Roldán; Norma A. Valdez-Cruz are members of the Sistema Nacional de Investigadores, Consejo Nacional de Ciencia y Tecnología. This work was supported by "Programa de Apoyo a Proyectos de Investigación e Innovación Tecnológica, Universidad Nacional Autónoma de México" [Grant No IN211422, IN210822]. This project was developed under the Institutional Program of the Instituto de Investigaciones Biomédicas UNAM: "La producción de biomoléculas de interés biomédico en bacterias y hongos". The funders had no role in data collection and analysis, decision to publish, or preparation of the manuscript.

Conflict of interest

NOP works in Probiomed S.A. de C.V., a company that manufactures recombinant human therapeutic proteins.

Acknowledgements

We thank Chem. Carlos Muñiz (Biosystems S.A. de C.V.) for technical assistance. We thank Dr. Carlos Calcines-Cruz and Dr. Alfonso López (Alvartis Pharma S.A. de C.V.) for technical support. We thank M. Sc. Laura Maria Muñoz-Echeverri for the helpful discussion. Also, we thank Dr. Guadalupe Zavala from "Unidad de Microscopía Electrónica IBT-UNAM" for TEM equipment rental and image digitalization and analysis support.

Supplementary material

https://doi.org/10.1016/j.ejbt.2022.08.004.

References

[1] Ferrer-Miralles N, Villaverde A. Bacterial cell factories for recombinant protein production; expanding the catalogue. Microb Cell Fact 2013;12:113. https://doi.org/10.1186/1475-2859-12-113. PMid: 24245806.
[2] Cano-Garrido O, Rodríguez-Carmona E, Díez-Gil C, et al. Supramolecular organization of protein-releasing functional amyloids solved in bacterial inclusion bodies. Acta Biomater 2013;9(4):6134–42. https://doi.org/10.1016/j.actbio.2012.11.033. PMid: 23220450.
[3] Bhatwa A, Wang W, Hassan YI, et al. Challenges associated with the formation of recombinant protein inclusion bodies in Escherichia coli and strategies to address them for industrial applications. Front Bioeng Biotechnol 2021;9:630551. https://doi.org/10.3389/fbioe.2021.630551. PMid: 33644021.
[4] Calcines-Cruz C, Olvera A, Castro-Acosta RM. Recombinant-phospholipase A2 production and architecture of inclusion bodies are affected by pH in *Escherichia coli*. Int J Biol Macromol 2018;108:826–36. https://doi.org/10.1016/j.ijbiomac.2017.10.178. PMid: 29101045.
[5] Castellanos-Mendoza A, Castro-Acosta RM, Olvera A, et al. Influence of pH control in the formation of inclusion bodies during production of recombinant sphingomyelinase-D in *Escherichia coli*. Microb Cell Fact 2014;13:137. https://doi.org/10.1186/s12934-014-0137-9. PMid: 25213001.
[6] de Marco A, Ferrer-Miralles N, Garcia-Fruitós E, et al. Bacterial inclusion bodies are industrially exploitable amyloids. FEMS Microbiol Rev 2019;43(1):53–72. https://doi.org/10.1093/femsre/fuy038. PMid: 30357330.
[7] Kopp J, Slouka C, Strohmer D, et al. Inclusion body bead size in *E. coli* controlled by physiological feeding. Microorganisms 2018;6(4):116. https://doi.org/10.3390/microorganisms6040116. PMid: 30477255.
[8] Datta S. Optimizing granulocyte colony-stimulating factor transcript for enhanced expression in *Escherichia coli*. Front Bioeng Biotechnol 2021;9:630367. https://doi.org/10.3389/fbioe.2021.630367. PMid: 33768088.
[9] Slouka C, Kopp J, Hutwimmer S, et al. Custom made inclusion bodies: Impact of classical process parameters and physiological parameters on inclusion body quality attributes. Microb Cell Fact 2018;17(1):148. https://doi.org/10.1186/s12934-018-0997-5. PMid: 30236107.
[10] Slouka C, Kopp J, Spadiut O, et al. Perspectives of inclusion bodies for bio-based products: Curse or blessing? Appl Microbiol Biotechnol 2019;103:1143–53. https://doi.org/10.1007/s00253-018-9569-1. PMid:30569219.
[11] García-Fruitós E, Vázquez E, Díez-Gil C, et al. Bacterial inclusion bodies: Making gold from waste. Trends Biotechnol 2012;30(2):65–70. https://doi.org/10.1016/j.tibtech.2011.09.003. PMid: 22037492.
[12] Ramón A, Señorale-Pose M, Marín M. Inclusion bodies: Not that bad. . .. Front Microbiol 2014;5:56. https://doi.org/10.3389/fmicb.2014.00056. PMid: 24592259.
[13] Gutiérrez-González M, Farías C, Tello S, et al. Optimization of culture conditions for the expression of three different insoluble proteins in *Escherichia coli*. Sci Rep 2019;9:16850. https://doi.org/10.1038/s41598-019-53200-7. PMid: 31727948.
[14] Pesarrodona M, Jauset T, Díaz-Riascos ZV, et al. Targeting antitumoral proteins to breast cancer by local administration of functional inclusion bodies. Adv Sci (Weinh) 2019;6(18):1900849. https://doi.org/10.1002/advs.201900849. PMid: 31559131.
[15] Singhvi P, Saneja A, Srichandan S, et al. Bacterial inclusion bodies: A treasure trove of bioactive proteins. Trends Biotechnol 2020;38(5):474–86. https://doi.org/10.1016/j.tibtech.2019.12.011. PMid: 31954528.
[16] Sánchez JM, López-Laguna H, Álamo P, et al. Artificial inclusion bodies for clinical development. Adv Sci 2019;7(3):1902420. https://doi.org/10.1002/advs.201902420. PMid: 32042562.
[17] Dhanker R, Hussain T, Tyagi P, et al. The emerging trend of bio-engineering approaches for microbial nanomaterial synthesis and its applications. Front Microbiol 2021;12:638003. https://doi.org/10.3389/fmicb.2021.638003. PMid: 33796089.
[18] Restrepo-Pineda S, Pérez NO, Valdez-Cruz NA, et al. Thermoinducible expression system for producing recombinant proteins in Escherichia coli: Advances and insights. FEMS Microbiol Rev 2021;45(6):fuab023. https://doi.org/10.1093/femsre/fuab023. PMid: 33844837.
[19] Valdez-Cruz NA, Caspeta L, Pérez NO, et al. Production of recombinant proteins in *E. coli* by the heat-inducible expression system based on the phage lambda pL and/or pR promoters. Microb Cell Fact 2010;9:18. https://doi.org/10.1186/1475-2859-9-18. PMid: 20298615.
[20] Caspeta L, Lara AR, Pérez NO, et al. Enhancing thermo-induced recombinant protein production in *Escherichia coli* by temperature oscillations and post-induction nutrient feeding strategies. J Biotechnol 2013;167(1):47–55. https://doi.org/10.1016/j.jbiotec.2013.06.001. PMid: 23792780.
[21] Mateus A, Bobonis J, Kurzawa N, et al. Thermal proteome profiling in bacteria: Probing protein state in vivo. Mol Syst Biol 2018;14(7):e8242. https://doi.org/10.15252/msb.20188242. PMid: 29980614.
[22] Valdez-Cruz NA, Ramírez OT, Trujillo-Roldán MA. Molecular responses caused by the production of recombinant proteins in the heat inducible expression system: *E. coli* with lambda phage pL and/or pR promoters. Bioeng Bugs 2011;2(2):105–10. https://doi.org/10.4161/bbug.2.2.14316. PMid: 21636998.
[23] Jazini M, Herwig C. Effects of temperature shifts and oscillations on recombinant protein production expressed in *Escherichia coli*. Bioprocess Biosyst Eng 2013;36(11):1571–7. https://doi.org/10.1007/s00449-013-0927-1. PMid: 23423557.

[24] de Groot NS, Ventura S. Effect of temperature on protein quality in bacterial inclusion bodies. FEBS Lett 2006;580(27):6471–6. https://doi.org/10.1016/j.febslet.2006.10.071. PMid: 17101131.
[25] Peternel Š, Grdadolnik J, Gaberc-Porekar V, et al. Engineering inclusion bodies for non-denaturing extraction of functional proteins. Microb Cell Fact 2008;7(1):34. https://doi.org/10.1186/1475-2859-7-34. PMid: 19046444.
[26] Hayat SM, Farahani N, Golichenari B, et al. Recombinant protein expression in Escherichia coli (*E. coli*): What we need to know. Curr Pharma Des 2018;24(6):718–25. https://doi.org/10.2174/1381612824666180131121940. PMid: 29384059.
[27] Wu R, Cao J, Liu F, et al. High-level soluble expression of phospholipase D from *Streptomyces chromofuscus* in *Escherichia coli* by combinatorial optimization. Electron J Biotechnol 2021;50:1–9. https://doi.org/10.1016/j.ejbt.2020.12.002.
[28] Strandberg L, Enfors SO. Factors influencing inclusion body formation in the production of a fused protein in *Escherichia coli*. Appl Environ Microbiol 1991;57(6):1669–74. https://doi.org/10.1128/aem.57.6.1669-1674.1991. PMid: 1908208.
[29] Valax P, Georgiou G. Molecular characterization of β-Lactamase inclusion bodies produced in *Escherichia coli*. 1. Composition. Biotechnol Prog 1993;9(5):539–47. https://doi.org/10.1021/bp00023a014. PMid: 7764166.
[30] Restrepo-Pineda S, Bando-Campos CG, Valdez-Cruz NA, et al. Recombinant production of ESAT-6 antigen in thermoinducible *Escherichia coli:* The role of culture scale and temperature on metabolic response, expression of chaperones, and architecture of inclusion bodies. Cell Stress Chaperon 2019;24:777–92. https://doi.org/10.1007/s12192-019-01006-x. PMid: 31165436.
[31] Singh A, Upadhyay V, Singh A, et al. Structure-Function relationship of inclusion bodies of a multimeric protein. Front Microbiol 2020;11:876. https://doi.org/10.3389/fmicb.2020.00876. PMid: 32457730.
[32] Metcalf D. The colony-stimulating factors and cancer. Cancer Immunol Res 2013;1(6):351–6. https://doi.org/10.1158/2326-6066.CIR-13-0151. PMid: 24524092.
[33] Ho JG, Middelberg AP. Estimating the potential refolding yield of recombinant proteins expressed as inclusion bodies. Biotechnol Bioeng 2004;87(5):584–92. https://doi.org/10.1002/bit.20148. PMid: 15352056.
[34] Trapnell BC, Inoue Y, Bonella F, et al. Inhaled Molgramostim therapy in autoimmune pulmonary alveolar proteinosis. N Engl J Med 2020;383(17):1635–44. https://doi.org/10.1056/NEJMoa1913590. PMid: 32897035.
[35] Lang FM, Lee KMC, Teijaro JR, et al. GM-CSF-based treatments in COVID-19: Reconciling opposing therapeutic approaches. Nat Rev Immunol 2020;20:507–14. https://doi.org/10.1038/s41577-020-0357-7. PMid: 32576980.
[36] Walter MR, Cook WJ, Ealick SE, et al. Three-dimensional structure of recombinant human granulocyte-macrophage colony-stimulating factor. J Mol Biol 1992;224(4):1075–85. https://doi.org/10.1016/0022-2836(92)90470-5.
[37] Burgess AW, Begley CG, Johnson GR, et al. Purification and properties of bacterially synthesized human granulocyte-macrophage colony stimulating factor. Blood 1987;69(1):43–51. https://doi.org/10.1182/blood.V69.1.43.43. PMid: 3024761.
[38] Rinas U, Hoffmann F, Betiku E, et al. Inclusion body anatomy and functioning of chaperone-mediated in vivo inclusion body disassembly during high-level recombinant protein production in *Escherichia coli*. J Biotechnol 2007;127(2):244–57. https://doi.org/10.1016/j.jbiotec.2006.07.004. PMid: 16945443.
[39] Wittmann C, Weber J, Betiku E, et al. Response of fluxome and metabolome to temperature-induced recombinant protein synthesis in *Escherichia coli*. J Biotechnol 2007;132(4):375–84. https://doi.org/10.1016/j.jbiotec.2007.07.495. PMid: 17689798.
[40] Restrepo-Pineda S, Sánchez-Puig N, Pérez NO, et al. The pre-induction temperature affects recombinant HuGM-CSF aggregation in thermoinducible *Escherichia coli*. Appl Microbiol Biotechnol 2022;106:2883–902. https://doi.org/10.1007/s00253-022-11908-z. PMid: 35412129.
[41] Giansanti P, Tsiatsiani L, Low T, et al. Six alternative proteases for mass spectrometry–based proteomics beyond trypsin. Nat Protoc 2016;11:993–1006. https://doi.org/10.1038/nprot.2016.057. PMid: 27123950.
[42] Rodríguez-Carmona E, Cano-Garrido O, Seras-Franzoso J, et al. Isolation of cell-free bacterial inclusion bodies. Microb Cell Fact 2010;9:71. https://doi.org/10.1186/1475-2859-9-71. PMid: 20849629.
[43] Haddad L, Babaeipour V, Mofid MR. The effect of cell disruption techniques and chaotropic agents on the downstream purification process of mecasermin produced as inclusion body in *E. coli*. Res Pharm Sci 2015;10(6):553–61.
[44] Pérez-Rodriguez S, Ramírez-Lira M, Wulff T, et al. Enrichment of microsomes from Chinese hamster ovary cells by subcellular fractionation for its use in proteomic analysis. PLoS ONE 2020;15(8):e0237930. https://doi.org/10.1371/journal.pone.0237930. PMid: 32841274.
[45] Hempelmann E, Krafts K. The mechanism of silver staining of proteins separated by SDS polyacrylamide gel electrophoresis. Biotech Histochem 2017;92(2):79–85. https://doi.org/10.1080/10520295.2016.1265149. PMid: 28296548.
[46] Zandomeneghi G, Krebs MR, McCammon MG, et al. FTIR reveals structural differences between native β-sheet proteins and amyloid fibrils. Protein Sci 2004;13(12):3314–21. https://doi.org/10.1110/ps.041024904. PMid: 15537750.
[47] Natalello A, Doglia SM. Insoluble protein assemblies characterized by Fourier transform infrared spectroscopy. In: García-Fruitós E, editor. Insoluble proteins. Methods in molecular biology (methods and protocols). New York, NY: Humana Press; 2015. p. 347–69. https://doi.org/10.1007/978-1-4939-2205-5_20. PMid: 25447875.
[48] Upadhyay AK, Murmu, Singh A, et al. Kinetics of inclusion body formation and its correlation with the characteristics of protein aggregates in Escherichia coli. PLoS One 2012;7. https://doi.org/10.1371/journal.pone.0033951. PMid: 22479486.
[49] Huber HE, Edwards G, Goodhart PJ, et al. Transcription factor E2F binds DNA as a heterodimer. PNAS 1993;90(8):3525–9. https://doi.org/10.1073/pnas.90.8.3525. PMid: 8475102.
[50] Luviano A, Cruz-Castañeda R, Sánchez-Puig N, et al. Cooperative energetic effects elicited by the yeast Shwachman-Diamond syndrome protein (Sdo1) and guanine nucleotides modulate the complex conformational landscape of the elongation factor-like 1 (Efl1) GTPase. Biophys Chem 2019;247:13–24. https://doi.org/10.1016/j.bpc.2019.02.003. PMid: 30780079.
[51] Louis-Jeune C, Andrade-Navarro MA, Perez-Iratxeta C. Prediction of protein secondary structure from circular dichroism using theoretically derived spectra. Proteins 2012;80(2):374–81. https://doi.org/10.1002/prot.23188. PMid: 22095872.
[52] O'Beirne D, Hamer G. The utilization of glucose/acetate mixtures by *Escherichia coli* W3110 under aerobic growth conditions. Bioprocess Eng 2000;23(4):375–80. https://doi.org/10.1007/s004499900176.
[53] Anane E, Lopez DC, Neubauer P, et al. Modelling overflow metabolism in *Escherichia coli* by acetate cycling. Biochem Eng J 2017;125:23–30. https://doi.org/10.1016/j.bej.2017.05.013.
[54] Kim S, Kim Y, Suh DH, et al. Heat-responsive and time-resolved transcriptome and metabolome analyses of *Escherichia coli* uncover thermo-tolerant mechanisms. Sci Rep 2020;10(1):17715. https://doi.org/10.1038/s41598-020-74606-8. PMid: 33077799.
[55] Valdez-Cruz NA, Reynoso-Cereceda GI, Pérez-Rodriguez S, et al. Production of a recombinant phospholipase A2 in *Escherichia coli* using resonant acoustic mixing that improves oxygen transfer in shake flasks. Microb Cell Fact 2017;16(1):129. https://doi.org/10.1186/s12934-017-0746-1. PMid: 28743267.
[56] Shivu B, Seshadri S, Li J, et al. Distinct beta-sheet structure in protein aggregates determined by ATR-FTIR spectroscopy. Biochem 2013;52(31):5176–83. https://doi.org/10.1021/bi400625v. PMid: 23837615.
[57] Yushchenko T, Deuerling E, Hauser K. Insights into the aggregation mechanism of PolyQ proteins with different glutamine repeat lengths. Biophys J 2018;114(8):1847–57. https://doi.org/10.1016/j.bpj.2018.02.037. PMid: 29694863.
[58] Biancalana M, Makabe K, Koide A, et al. Aromatic cross-strand ladders control the structure and stability of beta-rich peptide self-assembly mimics. J Mol Biol 2008;383(1):205–13. https://doi.org/10.1016/j.jmb.2008.08.031. PMid: 18762191.
[59] Singh A, Upadhyay V, Upadhyay AK, et al. Protein recovery from inclusion bodies of *Escherichia coli* using mild solubilization process. Microb Cell Fact 2015;14:41. https://doi.org/10.1186/s12934-015-0222-8. PMid: 25889252.
[60] Park A-R, Jang S-W, Kim J-S, et al. Efficient recovery of recombinant CRM197 expressed as inclusion bodies in *E. coli*. PLoS ONE 2018;13(7):e0201060. https://doi.org/10.1371/journal.pone.0201060. PMid: 30021008.
[61] Mansey MS, Ghareeb KA, Moghazy AN, et al. Glucose concentration affects recombinant interferon α-2b production in *Escherichia coli* using thermo-induction system. J Appl Pharm Sci 2014;4:1–5. https://doi.org/10.7324/JAPS.2014.40501.
[62] Singha TK, Gulati P, Kumar S. Nonconventional induction strategies for production of recombinant human tumor necrosis factor-alpha in *Escherichia coli*. J App Biol Biotechnol 2018;6(1):23–7. https://doi.org/10.7324/JABB.2018.60105.
[63] Wallace EW, Kear-Scott JL, Pilipenko EV, et al. Reversible, specific, active aggregates of endogenous proteins assemble upon heat stress. Cell 2015;162(6):1286–98. https://doi.org/10.1016/j.cell.2015.08.041. PMid: 26359986.
[64] Leone S, Sannino F, Tutino ML, et al. Acetate: Friend or foe? Efficient production of a sweet protein in *Escherichia coli* BL21 using acetate as a carbon source. Microb Cell Fact 2015;14:106. https://doi.org/10.1186/s12934-015-0299-0. PMid: 26208726.
[65] Adachi M, So M, Sakurai K, et al. Supersaturation limited, and unlimited phase transitions compete to produce the pathway complexity in amyloid fibrillation. J Biol Chem 2015;290(29):18134–45. https://doi.org/10.1074/jbc.M115.648139. PMid: 26063798.
[66] Macdonald RD, Khajehpour M. Effects of the protein denaturant guanidinium chloride on aqueous hydrophobic contact-pair interactions. Biophys Chem 2015;196:25–32. https://doi.org/10.1016/j.bpc.2014.08.006. PMid: 25268875.